



Evaluation of groundwater potential, aquifer parameters and vulnerability using geoelectrical method: a case study of parts of the Sanaga Maritime Division, Douala, Cameroon

Raymond Soweh Mbinkong¹ · Serge Hugues Pokam Kengni¹ · Ndikum Eric Ndoh^{2,3} ·
Tepoule Dongmo Narcisse Gaetan⁴ · Blaise Pascal Gounou Pokam⁴ · Charles Tabod Tabod^{1,4}

Received: 18 July 2023 / Accepted: 16 December 2023 / Published online: 20 January 2024
© The Author(s), under exclusive licence to Springer Nature Switzerland AG 2023

Abstract

A geoelectric survey was carried out in parts of the Sanaga maritime division where the limited quality of surface water sources, insufficient geophysical knowledge and a growing population have had a significant impact on the assessment and development of groundwater in the area. Forty-six vertical electrical soundings (VES) involving the Schlumberger electrode configuration were carried out across the study area to assess the groundwater potential and vulnerability which will assist in the proper siting of wells/boreholes. The VES survey was carried out using the ABEM SAS 1000 instrument with a maximum current electrode spread (AB/2) of 120 m. Field data obtained were curve-matched and iterated using the JOINTEM software to estimate groundwater repositories. The modelling results revealed three to five geoelectric layers including the topsoil, laterite, weathered formation, cracked gneiss and gneiss. VES curves obtained included the A, AA, H, HA, HK, HKH, KH, KHK, and QH. A correlation between borehole logs and the VES lithology was made and is in agreement. The aquifer unit was identified at the third and fourth geoelectric layers with thickness and resistivity ranging from 18 to 47 m and 93–16500 Ωm , respectively. The evaluated aquifer parameters (longitudinal conductance, transverse resistance, hydraulic conductivity, transmissivity, reflection coefficient and fracture contrast) ranged: 0.0026 to 0.28 mhos, 1981 to 702,405 Ωm^2 , 0.05 to 5.67 m/day, 2–150 m^2/day , -0.67 to 0.93, and 0.19 to 29, respectively. Contour maps were drawn from the estimated aquifer parameters to show their distribution in the study area, from which groundwater potential areas were delineated. The distribution of longitudinal conductance showed poor to moderate protective capacity throughout the study area. The findings of this study hold significant value as a reference for guiding groundwater exploration and development activities in the study area.

Keywords Sanaga maritime · Aquifer · VES · Resistivity · Groundwater potential

Introduction

The development of any community is dependent on access to basic amenities like good roads, electricity supply and water. Water is essential for the survival of all living things (Vuorinen et al. 2007) and is the most abundant and widely used component on Earth (Chow et al. 1988). While water is indeed abundant in nature, accessing it in sufficient quantity and quality remains a principal challenge (Salako et al. 2009; Sirhan et al. 2011). The issue becomes particularly critical in urban and peri-urban areas, where human activities are significant contributors to the contamination of surface water (Koji et al. 2017). The area under study is a peri-urban centre characterized by bustling economic activities, including agriculture, forest exploitation, fishing, and various industries. The region is confronted with a significant challenge regarding access to safe drinking water due

✉ Raymond Soweh Mbinkong
mbinkongraymond@gmail.com

¹ Department of Physics, Faculty of Science, The University of Bamenda, Bamenda, Cameroon

² Department of Physics, Higher Teacher Training College (HTTC) Bambili, The University of Bamenda, Bamenda, Cameroon

³ Department of Fundamental Sciences, Higher Technical Teacher Training College (HTTTC) Bambili, The University of Bamenda, Bamenda, Cameroon

⁴ Department of Physics, Faculty of Science, University of Yaounde I, Yaounde, Cameroon

to the absence of a sustainable water supply network. While surface water sources such as rivers, streams, lakes and ponds, are available for the local population, they prove to be inadequate solutions as they are seasonal, unreliable, and often of poor quality (Tepoule et al. 2022). Surface waters are susceptible to contamination from surface processes, such as the discharge of chemicals and leaching from waste dumps into water bodies. These contaminants contribute to the spread of waterborne diseases, some of which can be fatal (Konwea and Ajayi 2021; Konwea et al. 2023). Consequently, there is a high demand for groundwater as a potential and sustainable alternative to overcome water-related challenges of the local population and improve access to a reliable and safe water supply.

Groundwater is obtainable in aquifers, which are water-bearing permeable rocks found beneath the earth's surface (Bello et al. 2019; Kirsch 2009). Groundwater is recommended for its natural microbiological quality and overall chemical quality, making it suitable for various purposes. It is a relatively safe and reliable source of drinking water in both rural and urban areas (Adeyemo et al. 2017), requiring little or no disinfection before use (Obiora et al. 2016). However, groundwater can be susceptible to pollutants from anthropogenic sources, which are transported along its flow path. Successful groundwater exploration therefore requires a sufficient understanding of the characteristics of the subsurface aquifers. In a basement complex, such as the current study area, groundwater is commonly located within fractured and weathered formations, acting as aquifer formations. Its distribution is not uniform and can be confined to specific zones or pockets within these fractured and weathered formations (Dan-Hassan and Olorunfemi 1999; Datta et al. 2020; Mogaji and Omobude 2017; Olorunfemi and Fasuyi 1993). Hence, good knowledge of the aquifer's hydraulic parameters, such as transmissivity, transverse resistance, longitudinal conductance, hydraulic conductivity, reflection coefficient, fracture contrast, and more, is crucial for the successful exploration, exploitation, and management of groundwater resources (Evans et al. 2010; George et al. 2016). The spatial variability of these aquifer properties due to geological heterogeneity emphasizes the importance of acquiring a deep understanding of them, as they play a significant role in determining the capacity and potential of aquifer reservoirs (George et al. 2015; Ekanem et al. 2020). The electrical resistivity method is an ancient geophysical exploration technique that has been widely used in groundwater exploration. It is a non-invasive technique used for probing depths in the subsurface. This method has been demonstrated by numerous authors that conducting electrical resistivity surveys is crucial for achieving long-lasting boreholes and ensuring a sustainable supply of water (Abdelrahman et al. 2023; Dhinsa et al. 2022; Ebong et al.

2021; Eugene-Okorie et al. 2020; Iserhien-Emekeme et al. 2017; Olabanji et al. 2019; Omosuyi et al. 2020; Rajendran et al. 2020; Rodrigue et al. 2022). Among the numerous electrode configurations used in resistivity measurements, the vertical electrical sounding (VES) technique with Schlumberger electrode configuration is highly preferred. This is because the VES technique is relatively fast, dependable and cost-effective in acquiring details of subsoil electrical characteristics. In addition, the instrumentation is simple, field logistics are easy and the analysis of data is less tedious and more direct when compared with other geophysical techniques (Ekine and Osobonye 1996; Zohdy et al. 1974). Parameters derived from VES measurements have proven to be valuable for planning and drilling groundwater wells. The lack of geophysical knowledge among individuals in the study area has resulted in unproductive boreholes, borehole failure, and contaminated groundwater with associated health risks. This study is aimed at evaluating the geoelectric and hydraulic parameters, as well as the aquifer potential in the study area to guide the siting and development of productive wells and boreholes.

Location of study area and geology

The study was conducted within the Sanaga maritime division in the littoral region of Cameroon (Fig. 1). It is located between Latitude 3.55–4.6 °N and Longitude 10.08–11 °E with elevation ranging from 29 to 862 m from the west to the east respectively (Fig. 2). The Sanaga maritime division has a population of 162315 persons following the 2010 population statistics, with a total land area of 9311 km² (Noiha et al. 2015; Tchindjang et al. 2016). It is inhabited by the indigenous people of Malimba, Pongo-Songo, Bakoko or Elog Mpo'o, Bassa and Bonangasse, as well as several other ethnic groups from across Cameroon following rural and urban migration (Nzeket et al. 2019). These individuals depend mainly on agriculture, fishing, and timber exploitation as their primary source of income. The climate of the study area is warm, humid, and of the Equatorial Guinean type, characterized by significant rainfall. It is made up of two seasons: the rainy season and the dry season. The rainy season is longer and lasts from March to October while the dry season lasts from November to February, with some fluctuations from climate changes. The study area has a mean annual rainfall between 3000 and 4000 mm, a mean temperature of 28 °C and a mean humidity of 88% (Tonga et al. 2013). The relief consists of hills and valleys with gentle slopes. The soils in the area exhibit a ferrallitic composition characterized by a sandy-clayey and lateritic texture. They range in color from yellowish-brown to bright brown and are formed from the weathering

Fig. 1 Location map of the study area showing VES points

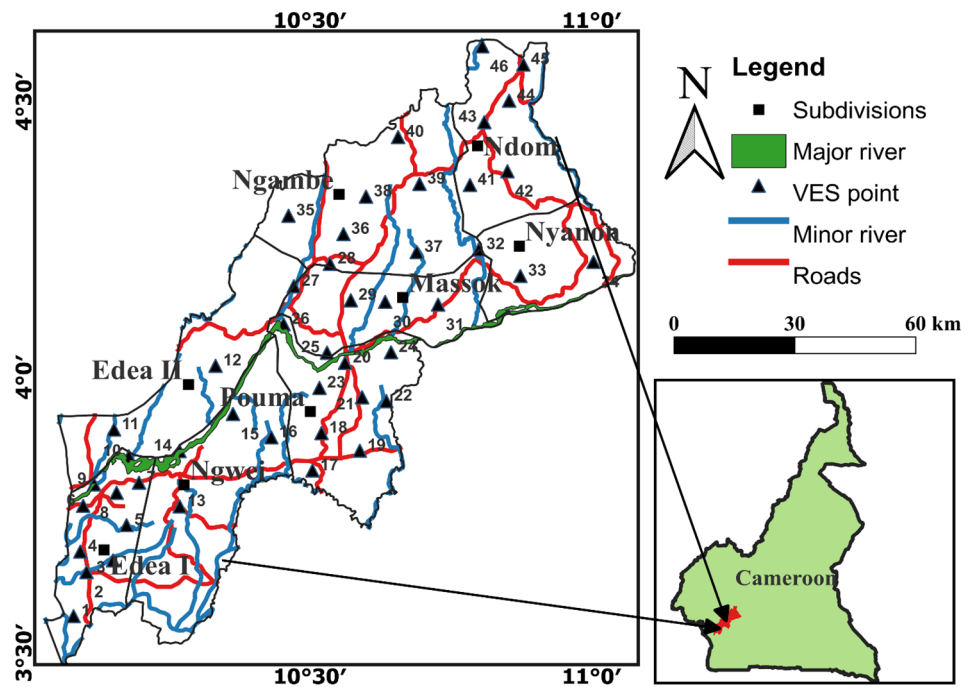
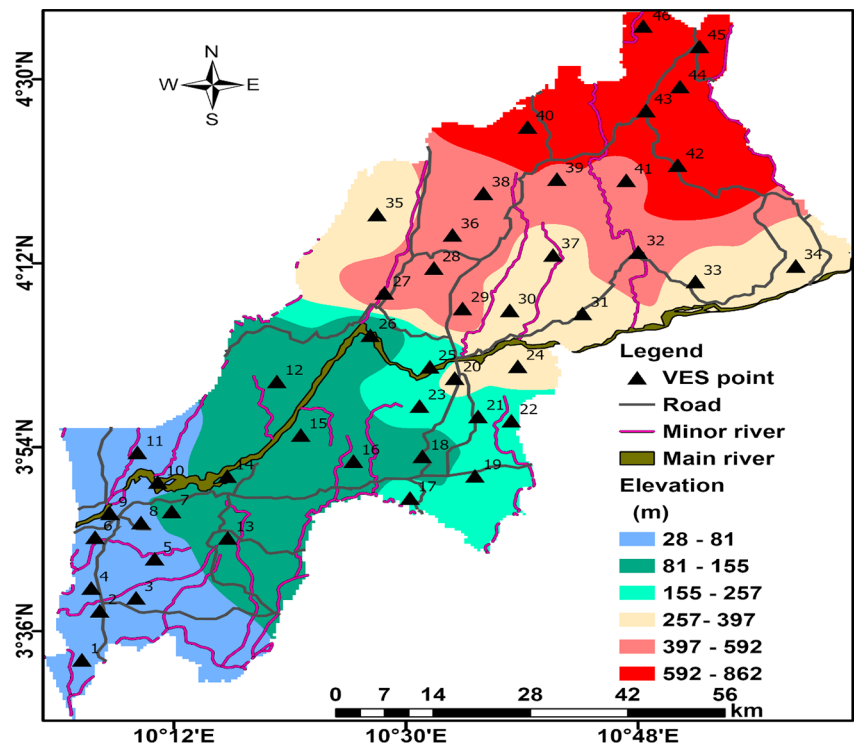


Fig. 2 Elevation map of the study area showing forty-six stations of measurement for VES



of underlying rocks (Nga et al. 2016; Tang et al. 2012). The study area is situated in the basement complexes of the Nyong unit (Bon et al. 2022; Lavenir et al. 2019) and the Yaounde group (Jude et al. 2021; Stendal et al. 2006). The geology of the study area is represented in Fig. 3. The Nyong unit is one among the three partitions of the Ntem complex, which includes the Ayna series, the Ntem and the Nyong unit (Teutsong et al. 2021). The Nyong unit is

situated in the northwestern part of the Ntem complex and is composed of metasedimentary and metavolcanic rocks, including syn to late-tectonic granitoids and syenites. These rocks have been discovered to result from high-grade metamorphism, dated at 2050 Ma (Lerouge et al. 2006). The prevalent rock types in the Nyong unit are biotite-hornblende gneisses with a composition of Tonalite-Trondhjemite-Granodiorite (TTG), orthopyroxene-garnet

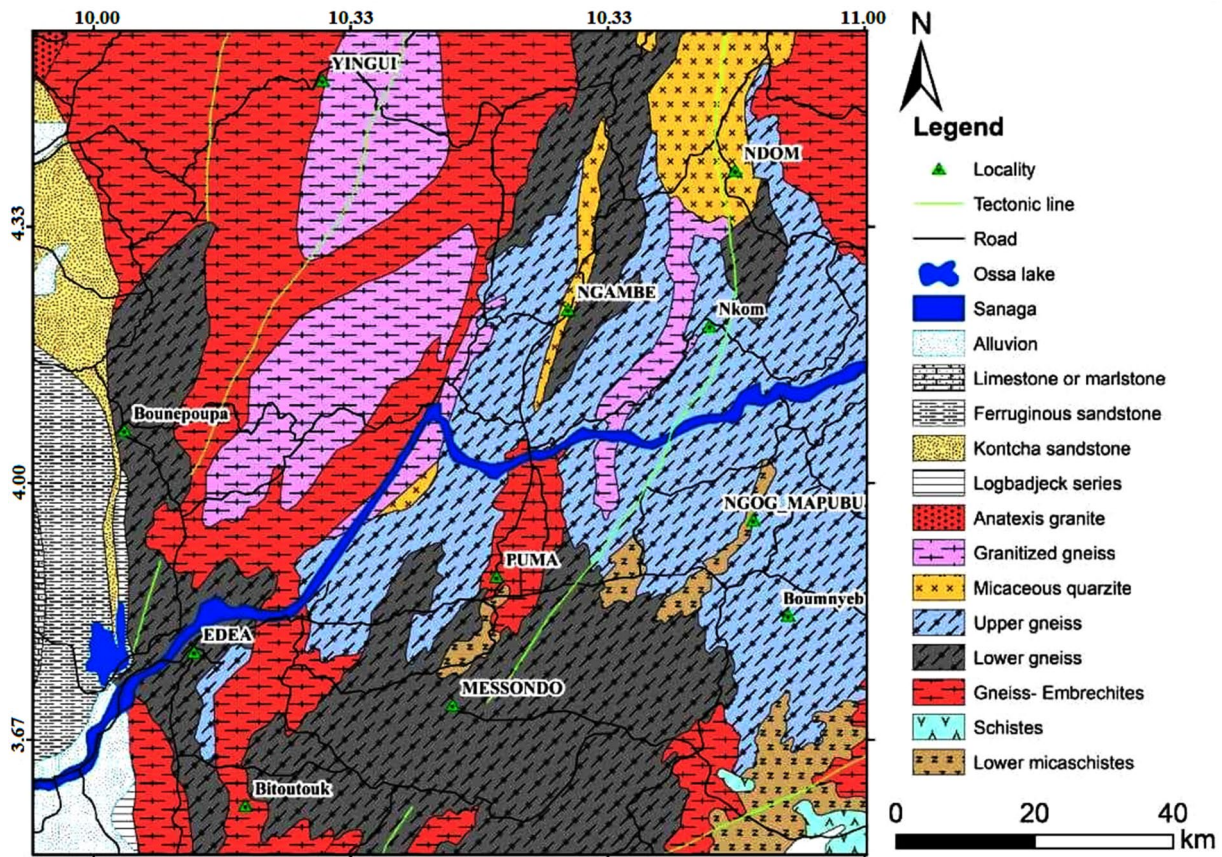


Fig. 3 Geological map of the study area (Dumort 1968)

gneisses (charnockites), garnet amphibole pyroxenites, and quartzites associated with banded iron formation (Nédélec et al. 1993; Shang et al. 2007; Toteu et al. 1994). Additionally, magmatic rocks such as syenites, granodiorites, and augen-metadiorites are also present (Mimba et al. 2014). The Yaoundé Group is situated in the southern area of the Central African Orogenic Belt (Bondje et al. 2020). It consists mainly of migmatites, granulites, and schists (Victor et al. 2014), which have been divided into two lithological units, namely, the meta-igneous and metasedimentary units (Toteu et al. 2006). The meta-igneous unit comprises pyroxenites, talcschists, and pyriclasites, while the metasedimentary unit is made up of kyanite-garnet gneiss, garnet-plagioclase gneiss, and garnet micaschist with calcisilicate rocks, quartzite, and talcschist intercalation (Stendal et al. 2006; Yonta-Ngoune et al. 2010).

Materials and methods

Forty-six VES were carried out in the study area using the Schlumberger electrode configuration. Data was collected following a geophysical campaign conducted in the study

area, using specific equipment for various measurements: The ABEM Terrameter SAS 1000 for resistivity measurement, measuring tape for taking distances, Global Positioning System (GPS) for taking coordinates and elevations of the VES points, electrical wires as electrode cables, two batteries to provide the DC source, crocodile clips to attach electrode cables to electrodes, and a hammer to send electrodes into the ground. The VES survey was conducted by arranging the four electrodes in a straight line. The potential electrodes (M, N) were positioned around a fixed center point of the array while symmetrically increasing the spacing of the current electrodes (A, B). This process resulted in a decreasing potential difference across M and N, eventually exceeding the measuring capabilities of the instrument. At this point, a new potential distance value was set, typically greater than the previous value. The direct current was introduced into the ground using the current electrodes and the resulting potential difference between the potential electrodes was measured. The half current electrode spacing ($AB/2$) was employed and systematically varied from 1 to 120 m. To reduce ambiguity in interpreting geoelectrical data, selected VES points were strategically positioned near existing boreholes in the

study area. This approach was implemented to enable a comparative analysis between the VES data and the information obtained from the borehole logs. The numerical value for the geometric factor (K) for each pair of the current and potential electrode spacing was determined using Eq. (1).

$$K = \pi \cdot \left[\frac{\left(\frac{AB}{2}\right)^2 - \left(\frac{MN}{2}\right)^2}{MN} \right] \tag{1}$$

where $MN/2$ is half the distance between potential electrodes and $AB/2$ is half the distance between the current electrodes.

The apparent resistivity (ρ_a) was obtained from the following equation:

$$\rho_a = KR \tag{2}$$

Where $R = \Delta V/I$ is the resistance, I is the current, and ΔV the potential difference between the two potential

electrodes. To analyze the field data, it was initially plotted on a bi-logarithmic graph, with the apparent resistivity on the vertical axis and the current electrode separation on the horizontal axis. The data was then smoothed to eliminate any traces of noise. The JOINTEM software was employed in modeling, iteration, and curve matching (Zohdy et al. 1974). The analysis yielded a good fit between the field data and modelled curves, with minimal root mean square (RMS) error. This successful fit provided accurate estimations of true resistivity, thickness, depth and the number of geoelectric layers for each VES (Fig. 4). The depth of investigation for each sounding curve was determined by taking into consideration the relationship between current electrode spacing and depth of investigation proposed by Roy and Apparao (1971). The resistivity and thickness of a given geoelectric layer establish the characteristics of a geoelectric unit and play a crucial role in the interpretation and understanding of geoelectric models. In the context of the aquifer unit, the resistivity and thickness values obtained from the model curves were used to estimate various parameters following the

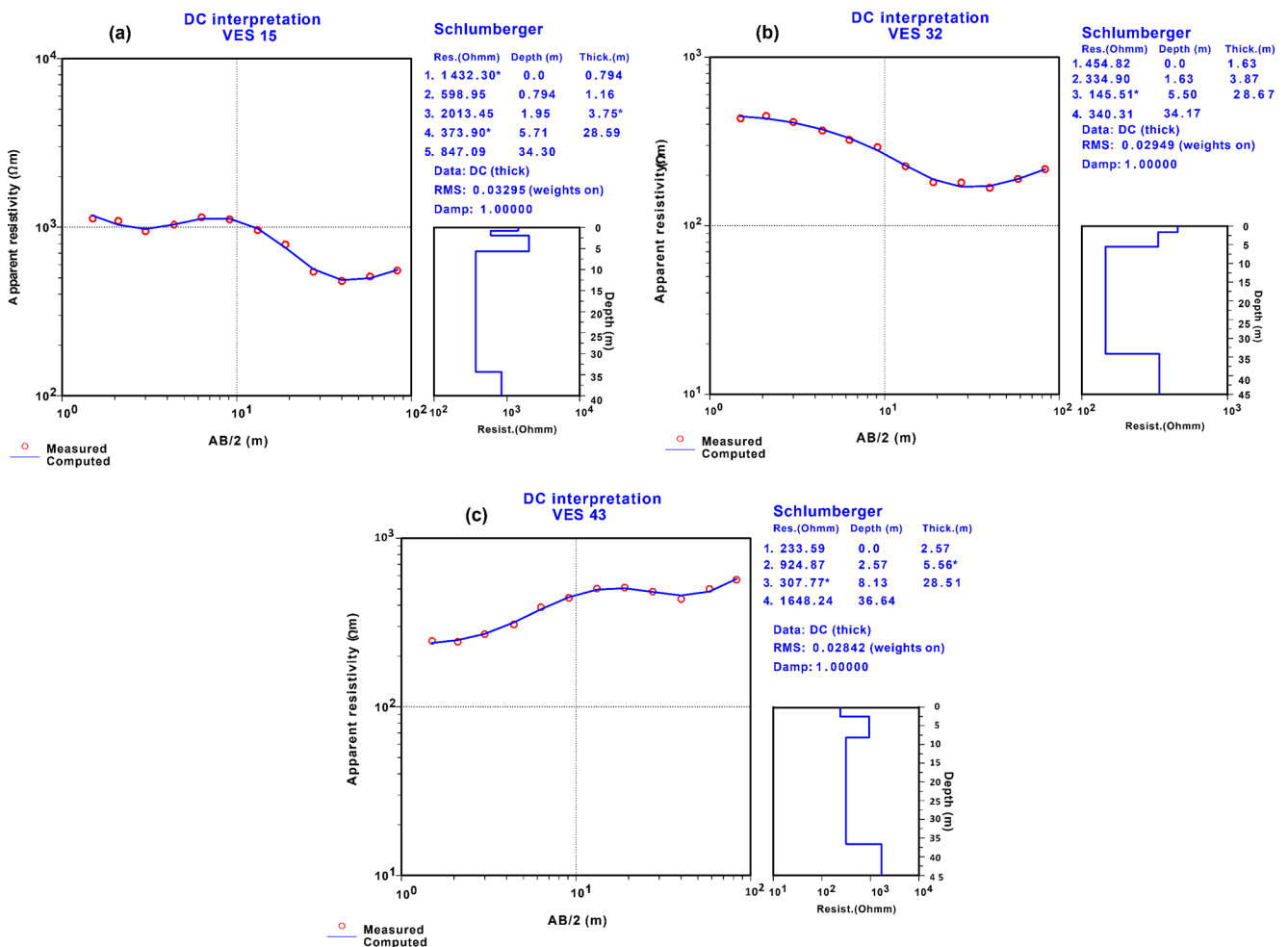


Fig. 4 Typical 1-D resistivity modelled curves a VES 15 b VES 32 c VES 43

Table 1 Aquifer protective capacity rating proposed by Oladapo and Akintorinwa (2007)

Longitudinal conductance (Ω^{-1})	Protective capacity rating
< 0.1	Poor
0.1–0.19	Weak
0.2–0.69	Moderate
0.7–4.9	Good
5–10	Very good
>10	Excellent

methodologies and approaches described in the works of Ekanem (2020), Raji and Abdulkadir (2020), Obiora et al. (2017), Oladunjoye et al. (2018) and Raji and Abdulkadir (2022), which are relevant due to their geological similarity to the study area. The estimated parameters included the Dar-Zarouk parameters, hydraulic conductivity, transmissivity, reflection coefficient, and fracture contrast. The Dar-Zarouk parameters specifically refer to the longitudinal conductance (S) and the transverse resistance (T) (Maillet 1947). For a given geologic unit having resistivity (ρ) and thickness (h), the longitudinal conductance was estimated using Eq. (3).

$$S = \frac{h}{\rho} \quad (3)$$

The transverse resistance was calculated by the following equation:

$$T = h\rho \quad (4)$$

The aquifer longitudinal conductance is important in determining its protective capacity against subsurface contamination. It measures the ability of the aquifer to hinder the vertical migration of contaminants through its thickness and resistivity characteristics. To determine the aquifer's vulnerability in the study area, the aquifer protective capacity rating suggested by Oladapo and Akintorinwa (2007) was used (Table 1). The hydraulic conductivity (K) measures the ease with which groundwater flows via the pore spaces and was calculated using the equation of Heigold et al. (1979). K serves as an indicator of the porous and fractured areas present in subsurface rocks, which allow the smooth flow of groundwater through the pore spaces (Ossai et al. 2023).

$$K = 386.4\rho_{aq}^{-0.93283} \quad (5)$$

where 386.4 and -0.93283 are constants, and ρ_{aq} is the resistivity of the aquifer in Ω m. The aquifer transmissivity (Tr), which establishes the relationship between the thickness

Table 2 Classification of transmissivity magnitude (Krasny 1993)

Class of transmissivity	Transmissivity	Aquifer potential rating	Groundwater supply potential
I	> 1000	Very high	Withdrawals of great regional importance
II	100–1000	High	Withdrawals of lesser regional importance
III	10–100	Moderate	Withdrawals for local water supply (small communities, plants, etc.)
IV	1–10	Low	Withdrawals for local water supply (private consumption, etc.)
V	0.1–1	Very low	Withdrawals for local water supply with limited consumption
VI	< 0.1	Impeccable	Sources for local water supply are difficult (if possible) to ensure

and the hydraulic conductivity was estimated using Eq. (6) suggested by Niwas and Singhal (1981). The transmissivity quantifies the ability of a geologic unit to transmit water through it under a hydraulic gradient.

$$T_r = K\sigma T = \frac{KS}{\sigma} = Kh \quad (6)$$

where S is the longitudinal conductance in mhos, T is the transverse resistance in Ωm^2 , σ is the electrical conductivity and K is the hydraulic conductivity. The evaluated transmissivity values were used to determine the aquifer potential of the study area following the classification of Krasny (1993) presented in Table 2.

The reflection coefficient (R_c) and fracture contrast (F_c) were evaluated using Eqs. (7) and (8), respectively (Olayinka 1996).

$$R_c = \frac{\rho_n - \rho_{n-1}}{\rho_n + \rho_{n-1}} \quad (7)$$

$$F_c = \frac{\rho_n}{\rho_{n-1}} \quad (8)$$

where ρ_n is the nth layer's resistivity identified as the aquifer layer and ρ_{n-1} is the layer resistivity that overlies the nth layer.

Results and discussion

Iso-Resistivity maps

The maps for lateral and horizontal fluctuations in apparent resistivity were generated at depths of investigation of 5.28 m ($AB/2 = 13.2$ m), 23.2 m ($AB/2 = 58$ m), and 33.2 m ($AB/2 = 83$ m) (Fig. 5). The maps display apparent resistivity values ranging from 92 to 11837 Ω m and were categorized into three domains: the resistive, the low-conductive and the conductive domains. The conductive domain is represented by low apparent resistivity (92–500 Ω m), the low-conductive domain is represented by moderate apparent resistivity (500–2000 Ω m), while the resistive domain corresponds to high apparent resistivity (2000–11837 Ω m).

Figure 5 reveals an uneven distribution of apparent resistivities throughout the study area, which may result from the flow of current in different lithological units.

At $AB/2 = 13.2$ m (Fig. 5a), a resistive domain is observed in the central part of the study area with some traces in the southwestern parts with a resistivity ranging from 2196 to 6472 Ω m and may reflect the presence of gneiss or quartzite. The conductive domain is more in the northwestern part and extends to the upper margin of the central part with resistivity ranging between 92 and 444 Ω m, which may reflect the presence of clayey sand or laterite. The low-conductive domain is widespread across the study area but primarily at the southwest-central with a resistivity that varies from 503 to 1786 Ω m and may reflect the presence of laterite. At $AB/2 = 58$ m (Fig. 5b), The resistive domain observed

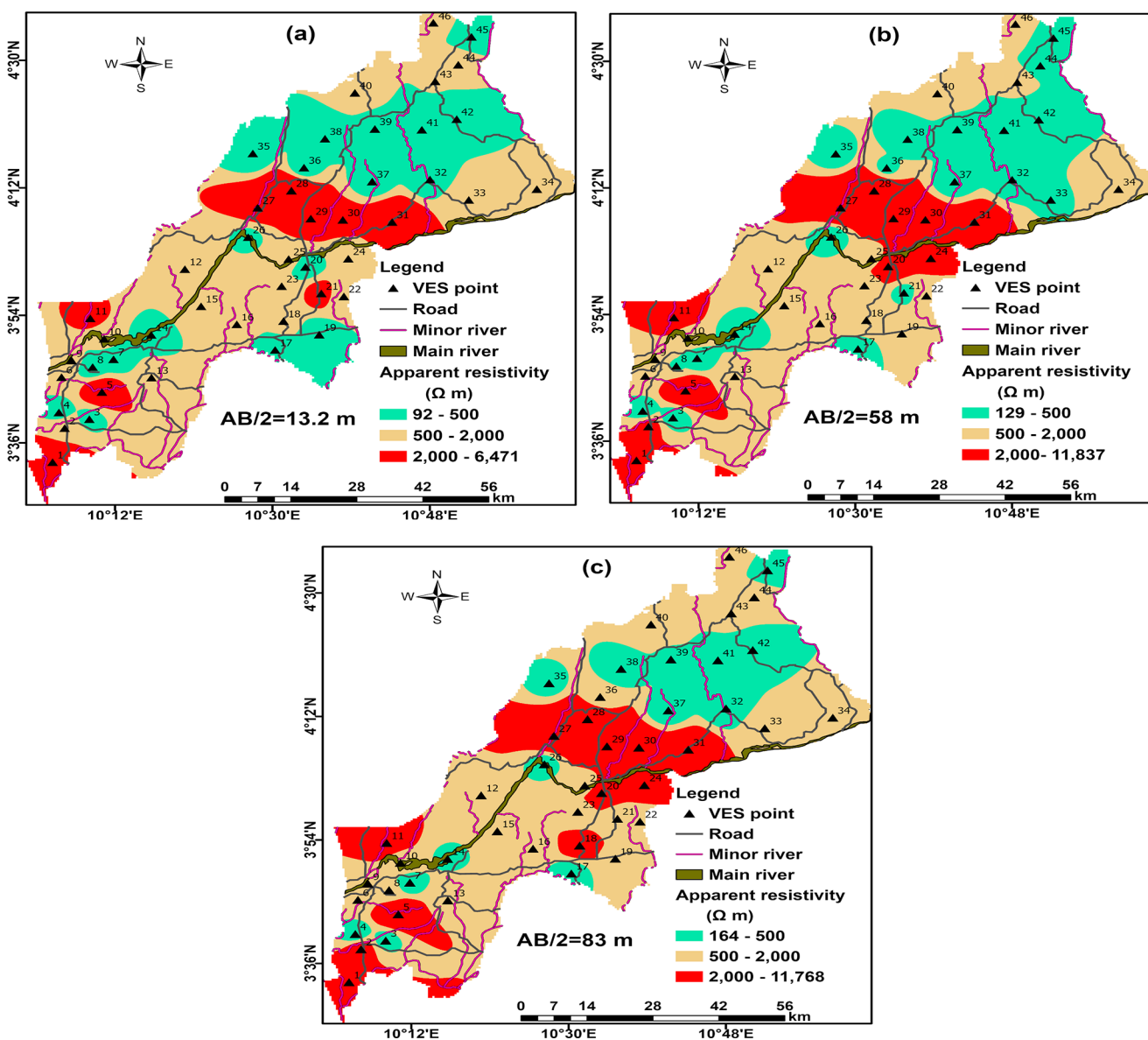


Fig. 5 Variations in apparent resistivity in the study area a $AB/2 = 13.2$ m b $AB/2 = 58$ m c $AB/2 = 83$ m

in previous depth (5.28 m) becomes more pronounced with high resistivity (3261–11,837 Ωm), indicating the existence of a healthy gneiss basement. Similarly, the conductive domain is highly pronounced in the northeastern part of the study area and spans from 142 to 483 Ωm . This could be attributed to the presence of a more or less weathered basement. The low-conductive domain varies from 535 to 1641 Ωm and could potentially be indicative of the presence of a more or less weathered basement. At $AB/2 = 83$ m (Fig. 5c), the resistive domain occupies the same pattern as in $AB/2 = 58$ m with resistivity that varies from 3836 to 11767 Ωm which could represent a fresh bedrock. The low-conductive domain shows an increase in resistivity (565–1789 Ωm) occupying more areas in the northeastern sector than at $AB/2 = 58$ m. This may represent the weathered basement with some fresh bedrock. The conductive domain spans from 264 to 474 Ωm and represents the weathered bedrock.

Goelectric and hydraulic parameters

The results from the modelling of VES data indicate sounding curves with 3 to 5 goelectric layers (Table 3). Specifically, VES 20, 28–30, 38, and 46 exhibit 3 layers, while VES 1–2, 5–10, 12–14, 16–19, 21–27, 31–37, 39–41, and 43–45 show 4 layers. Furthermore, VES 4, 11, 15, and 42 reveal the presence of 5 goelectric layers. Nine sounding curves were obtained and classified as A, AA, H, HA, HK, HKH, KH, KHK, and QH. The presence of such a diverse range of curves suggests the heterogeneous nature of the subsurface. The frequency distribution of these curves is depicted in Fig. 6, revealing the dominance of KH and QH curves. The first goelectric layer represents the topsoil and laterite topsoil with a resistivity and thickness that range between 106 and 1915 Ωm and 0.4–6 m, respectively. The second layer is characterized by laterite, clayey sand, gneiss and quartzite with a resistivity and thickness range of 60–9650 Ωm and 1–15 m, respectively. The third and fourth goelectric layers constitute the aquifer unit of the study area and represent the weathered formations with resistivity and thickness values that vary from 93 to 16500 Ωm and 18–47 m, respectively. The fifth goelectric layer was interpreted as the bedrock (fresh/weathered) and contains cracked gneiss and fresh gneiss material with resistivity values ranging from 144 to 16,601 Ωm and infinite thickness. The interpretation of geo-electric layers was guided by the analysis of lithologic logs obtained from boreholes in the study area. A correlation between the borehole logs and the VES curves lithology is in agreement (Fig. 7).

The spatial variation of aquifer resistivity across the study area is shown in Fig. 8. The aquifer resistivity ranges from 93 to 16500 Ωm with a mean value of 1722 Ωm . The distribution of aquifer resistivity reveals that the

northeastern sector and parts of the southwestern sector of the study area exhibit low resistive materials with values less than 500 Ωm , indicating the presence of water-bearing fractures with high conductive fluids. In contrast, the central sector is characterized by high resistivity, suggesting a low concentration of fluids. It can be inferred that this high resistive may be less suitable for accessing high-yield groundwater sources through drilling boreholes with high expectations of water productivity (Omosuyi 2010). The aquifer thickness varies between 18 and 47 m with an average value of 29 m. The observed variation in aquifer thickness can be attributed to a difference in the resistance of rocks to weathering. The contour map of aquifer thickness (Fig. 9) shows that the study area is significantly characterized by thick aquifers above 22 m, with the thickest aquifers mainly localized in the central and southwestern sectors of the study area. Thick aquifers provide a larger volume of rock material capable of storing and transmitting groundwater, which is essential for sustainable groundwater resources.

The Dar-Zarouk parameters, hydraulic conductivity, transmissivity, reflection coefficient and fracture contrast were obtained from the aquifer resistivity and thickness (Table 4). The Dar-Zarouk parameters were used to assess the aquifer's vulnerability to leachate contamination. The values of the longitudinal conductance were used to generate a contour map which gives the distribution of longitudinal conductance across the study area (Fig. 10). The longitudinal conductance in this study ranges from 0.0026 to 0.28 mhos, with an average value of 0.076 mhos. By comparing these values with the aquifer protective rating in Table 1, the study area can be classified into 3 different categories: poor, weak and moderate aquifer protective capacities. However, the spatial distribution of longitudinal conductance indicates that the study area predominantly falls within the poor to the weak range, accounting for approximately 63% and 24%, respectively. This suggests that the hydrogeological units in the study area are susceptible to contamination from surface sources. It is worth noting that there is an increasing trend in longitudinal conductance values from the central to the northeastern sector of the study area. Notably, the northeastern sector exhibits significantly higher longitudinal conductance values compared to other areas. This suggests that the aquifer protective capacity improves in the northeast, indicating a relatively lower susceptibility to surface source contamination in that particular area. The transverse resistance ranges from 1981 to 702405 Ωm^2 with a mean of 60809 Ωm^2 and is represented by the contour map in Fig. 11. The transverse resistance values obtained in this study are considerably lower than those obtained by Eugene-Okorie et al. (2020). The highest transverse resistance values are visible at the central and southwestern parts

Table 3 Summary of VES results

VES No	Curve type	No of layers	Resistivity($\rho_1/\rho_2/\dots/\rho_n$)	Thickness($h_1/h_2/\dots/h_n$)	Depth($p_1/p_2/\dots/p_n$)	Proposed lithology
1	KH	04	1665.66/5157.38/3285.03/9469.50	0.94/12.83/20.26	0.94/13.77/34.03	Laterite topsoil/ Gneiss/Weathered Formation/Gneiss
2	KH	04	610.59/5177.67/1513.78/8877.18	0.448/1.2/31.14	0.448/1.65/32.79	Topsoil/Gneiss/ Weathered Formation/Gneiss
3	HKH	05	591.26/267.79/667.83/230.37/1541.04	1.28/2.99/3.87/39.94	1.28/4.27/8.14/48.08	Topsoil/Clayey sand/Laterite/ Weathered Formation/Gneiss
4	HKH	05	277.50/177.44/463.94/168.85/143.81	1.75/2.11/3.42/26.33	1.75/3.86/7.28/33.61	Topsoil/Clayey sand/Laterite/ Weathered Formation /Cracked Gneiss
5	HA	04	2695.3/825.46/4749.93/6565.06	0.406/2.81/29.83	0.406/3.21/33.05	Quartzite/Laterite/ Weathered Formation /Gneiss
6	AA	04	1599.72/3261.74/5620.92/10943.96	1.019/6.90/40.08	1.019/7.92/48.00	Laterite topsoil/ Gneiss/ Weathered Formation /Gneiss
7	QH	04	287.67/160.61/96.74/850	5.67/10.85/18.42	5.67/16.52/34.94	Topsoil/Clayey Sand/Weathered Formation/cracked gneiss
8	HA	04	1122.02/488.15/1434.34/2827.84	0.422/6.38/26.25	0.422/6.8/33.06	Topsoil/ Laterite/ Weathered Formation /Gneiss
9	HK	04	564.30/100.71/1609.08/621.45	4.49/9.81/33.79	4.49/14.30/48.09	Topsoil/Clayey sand/Weathered Formation/ Cracked gneiss
10	QH	04	1097.22/621.28/525.2/10,022	0.454/4.57/28.08	0.454/5.02/33.1	Topsoil/Laterite/Weathered Formation/Gneiss
11	KHK	05	299.25/1159.54/189.81/2275.29/443.32	0.562/1.46/2.60/28.88	0.562/2.03/4.62/33.51	Topsoil/Laterite/ Clayey Sand/ Weathered Formation/Cracked gneiss
12	QH	04	3040.37/741.6/341/1690	0.435/11.52/21.75	0.435/11.96/33.71	Quartzite/Laterite/ Weathered Formation /Gneiss
13	QH	04	2972.98/690.94/517.34/8868.5	0.428/5/23.95	0.428/5.43/29.38	Quartzite/Laterite/Weathered Formation/Gneiss
14	QH	04	572.09/326.13/227.41/811.1	3.45/6.7/23.62	3.45/10.15/33.77	Topsoil/Clayey sand/Weathered Formation / Cracked Gneiss
15	HKH	05	1432.3/598.95/2013.45/373.9/847.09	0.794/1.16/3.75/28.59	0.794/1.95/5.71/34.30	Topsoil/Laterite/ Gneiss/Weathered Formation /cracked gneiss
16	QH	04	1303.25/2087.93/567.77/929.13	1.19/3.84/28.41	1.19/5.03/33.44	Topsoil/Gneiss/ Weathered Formation /cracked gneiss
17	HK	04	258.27/60.17/482.57/267.64	3.07/9.18/20.91	3.07/12.25/33.16	Topsoil/Clayey Sand/Weathered Formation / Cracked Gneiss

Table 3 (continued)

VES No	Curve type	No of layers	Resistivity($\rho_1/\rho_2/\dots/\rho_n$)	Thickness($h_1/h_2/\dots/h_n$)	Depth($p_1/p_2/\dots/p_n$)	Proposed lithology
18	HK	04	782.53/489.81/1213.22/617.38	1.14/2.35/29.67	1.14/3.49/33.16	Topsoil/Laterite/Weathered Formation /Cracked Gneiss
19	HA	04	178.59/113.03/3336.4/6562.85	2.81/4.35/40.81	2.81/7.15/47.97	Topsoil/Clayey sand/Gneiss / Gneiss
20	A	03	1853.89/16,500/18,446	5.66/42.57	5.66/48.22	Laterite topsoil/ Gneiss/Gneiss
21	QH	04	1619.17/652.48/347.7/2019.19	0.424/8.93/23.71	0.424/9.35/33.06	Topsoil/Laterite/Weathered Formation/Gneiss
22	KH	04	306.56/1740.36/316.29/8890.25	0.359/4.26/26.51	0.359/4.62/31.13	Topsoil/Laterite/Weathered Formation /Gneiss
23	KH	04	1914.58/2684.78/1514.3/16600.93	0.461/7.75/25.17	0.461/8.22/33.38	Laterite topsoil/ Quartzite/Weathered Formation / Gneiss
24	KH	04	249.53/739.77/325.72/1309.12	0.606/13.06/19.45	0.606/13.66/33.11	Topsoil/Laterite/Weathered Formation /Gneiss
25	AA	04	333.17/357.51/1600.49/3180.89	0.661/4.1/43.39	0.661/4.76/48.15	Topsoil/ Clayey sand/ Weathered Formation /Gneiss
26	QH	04	637.28/512.37/123.15/879.60	2.44/14.76/34.5	2.44/14.76/34.50	Topsoil/Laterite/Weathered Formation/ Cracked Gneiss
27	KH	04	278.22/10165.31/3634.66/15,000	0.877/18.01/29.13	0.877/18.89/48.02	Topsoil/Gneiss/ Weathered Formation/Gneiss
28	A	03	1657.13/9817.89/15285.7	1.36/46.69	1.36/48.05	Laterite topsoil/ Weathered Formation/Gneiss
29	A	03	583.91/6607.22/15639.4	1.44/31.58	1.44/33.01	Laterite topsoil/ Weathered Formation/Gneiss
30	A	03	842.66/2613.64/10128.96	0.84/32.05	0.84/32.89	Laterite topsoil/ Weathered Formation/Gneiss
31	KH	04	3914.54/9650.43/2768.98/1100 0.86	1.25/3.83/28.1	1.25/5.08/33.18	Quartzite/Gneiss/ Weathered Formation/Gneiss
32	QH	04	454.82/334.9/145.51/340.31	1.63/3.87/28.67	1.63/5.5/34.17	Laterite topsoil / Clayey sand/ Weathered Formation/ Cracked Gneiss
33	KH	04	889.51/1763.44/381.11/2096	1.86/4.40/27.82	1.86/6.26/34.09	Laterite topsoil/ Quartzite/Weathered Formation / Gneiss
34	KH	04	358.03/796.67/524.31/5552.97	1.14/3.33/28.09	1.14/4.47/32.56	Topsoil /Laterite/ Weathered Formation /Gneiss

Table 3 (continued)

VES No	Curve type	No of layers	Resistivity($\rho_1/\rho_2/\dots/\rho_n$)	Thickness($h_1/h_2/\dots/h_n$)	Depth($p_1/p_2/\dots/p_n$)	Proposed lithology
35	HK	04	355.43/161.46/535/265.94	2.8/5.43/24.79	2.8/8.23/33.02	Topsoil/Clayey Sand/Weathered Formation / Cracked Gneiss
36	KH	04	211.18/408.84/209.50/3102	2.73/11.90/18.09	2.73/14.63/32.72	Topsoil/Laterite/ Weathered Formation /Gneiss
37	QH	04	404.82/232.92/179.40/408.38	3.32/8.42/22.77	3.32/11.74/34.51	Topsoil/Clayey Sand/Weathered Formation / Cracked Gneiss
38	H	03	178.16/125.07/411.13	4.46/29.82	4.46/34.29	Topsoil/ Weathered Formation / Cracked Gneiss
39	KH	04	105.28/1516.53/316.63/639.92	0.612/1.47/31.99	0.612/2.08/34.07	Topsoil/Quartzite/ Weathered Formation /Cracked Gneiss
40	KH	04	310.59/849.43/553.13/6827	0.643/2.93/29.95	0.643/3.57/33.52	Topsoil/Laterite/ Weathered Formation /Gneiss
41	QH	04	255.2/195.85/104.86/942	1.7/13.13/21.82	1.7/14.83/36.65	Topsoil/Clayey Sand/ Weathered Formation / Cracked Gneiss
42	HKH	05	267.5/102.17/314.31/93.01/580.84	0.783/1.11/3.78/21.43	0.783/1.89/5.67/27.1	Topsoil/Clayey sand/Laterite and clay/Weathered Formation / Cracked Gneiss
43	KH	04	233.59/924.87/307.77/1648.24	2.57/5.56/28.51	2.57/8.13/36.64	Topsoil/ Laterite/ Weathered Formation /Gneiss
44	KH	04	119.41/801.8/270.1/1769.99	0.321/10.78/22.97	0.321/11.1/34.03	Topsoil/ Laterite/ Weathered Formation / Gneiss
45	QH	04	785.65/355.86/135.49/737.48	2.85/13.90/19.45	2.85/16.75/36.20	Laterite topsoil/ Clayey Sand/ Weathered Formation /Cracked Gneiss
46	A	03	299.02/612.30/1342.37	1.49/31.90	1.49/33.39	Topsoil/Weathered Formation/ Gneiss

of the study area while the lowest values are localised in the northeastern parts.

The distribution of hydraulic conductivity in the study area is represented by the contour map in Fig. 12 and spans a range from 0.05 to 5.67 m/day with a mean value of 1.63 m/day. The range of conductivity values obtained in this study is lower than those reported by Okpoli and Ozomoge (2020). Variations in hydraulic conductivity may be attributed to the inhomogeneity of facies change and variations in grain sizes within the aquifer system. Based on the range of hydraulic conductivity values observed in this study, the study area is demarcated into three zones: low (0.05–0.86 m/

day), moderate (0.86–3.7 m/day), and high (3.7–5.6 m/day) hydraulic conductivity zones. The high hydraulic conductivity zone is localized in the northeastern part of the study area with some traces in the central and southwestern regions. The moderate zone is widespread across the study area and accounts for 48% of the entire study area. The low zone is localized at the central and extreme southwestern parts of the study area. High hydraulic conductivity zones are associated with lower clay content, indicating greater permeability and ease of fluid flow (Heigold et al. 1979). The aquifer transmissivity values range from 2 to 150 m²/day with a mean value of 42.1 m²/day. These transmissivity values

Fig. 6 Frequency distribution of curve types in the study area showing the dominance of the KH and QK curves

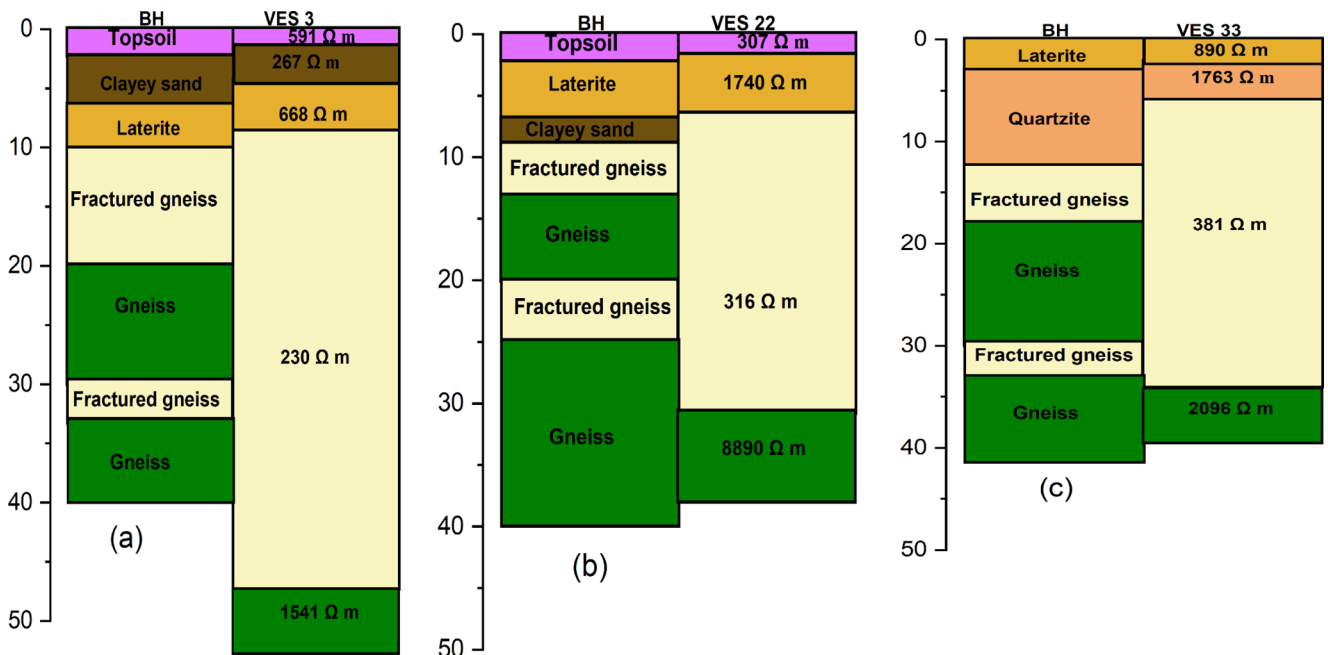
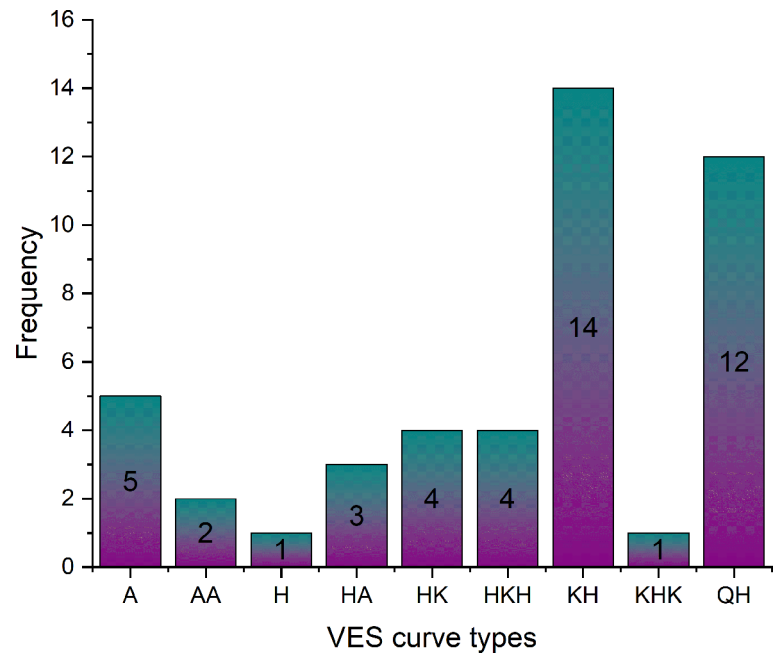


Fig. 7 Correlation between borehole litho-logs and VES stations **a** VES 3 **b** VES 22 **c** VES 33

correspond to a range of aquifer potential ratings suggested by Krasny (1993), which spans from low to high (Table 2). Following this classification, it is evident from Fig. 13 that 26%, 63% and 13% of the study area has low, moderate and high transmissivity, respectively. A comparison between the distribution of hydraulic conductivity and transmissivity reveals that areas of high transmissivity closely align with zones of high hydraulic conductivity and vice versa. As a result, it can be inferred that the aquifers located in the north-eastern part of the study area exhibit high permeability with

high water-bearing potential (Oguama et al. 2019). Figure 14 provides insight into the correlation between hydraulic conductivity and transmissivity. The plot illustrates a linear relationship, where higher values of transmissivity are observed to be associated with higher values of hydraulic conductivity. The strength of this correlation is indicated by a strong correlation coefficient of 0.908. Table 5 presents the results of borehole pumping tests conducted near certain VES points (VES 1, 3, 20, 22 and 30) in the study area. Their borehole yields range from 0.22 to 3.3 L/s reflecting variation in

Fig. 8 Contour map for aquifer resistivity showing its variation in the study area

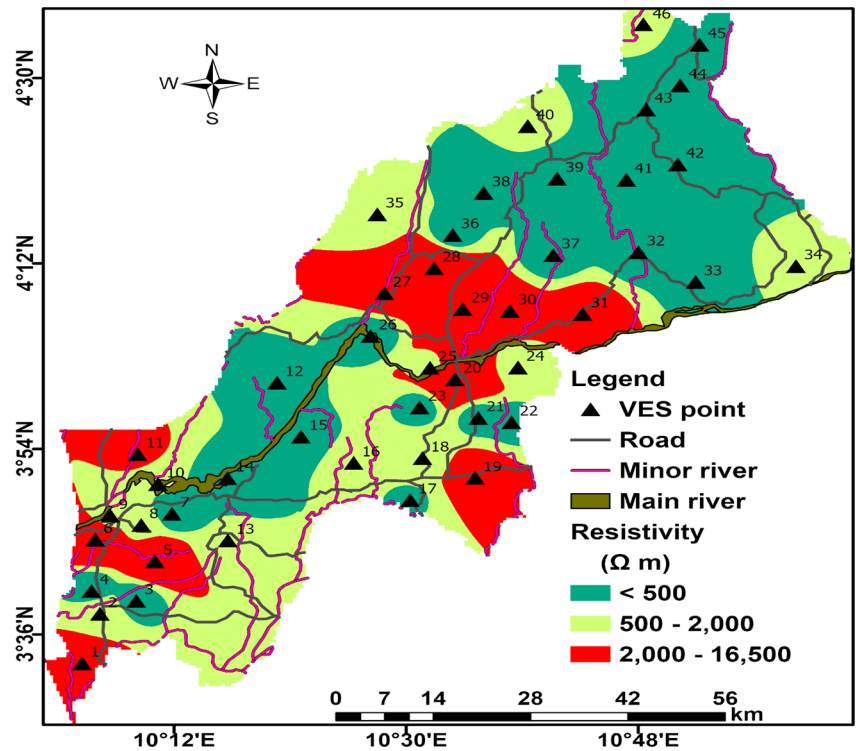
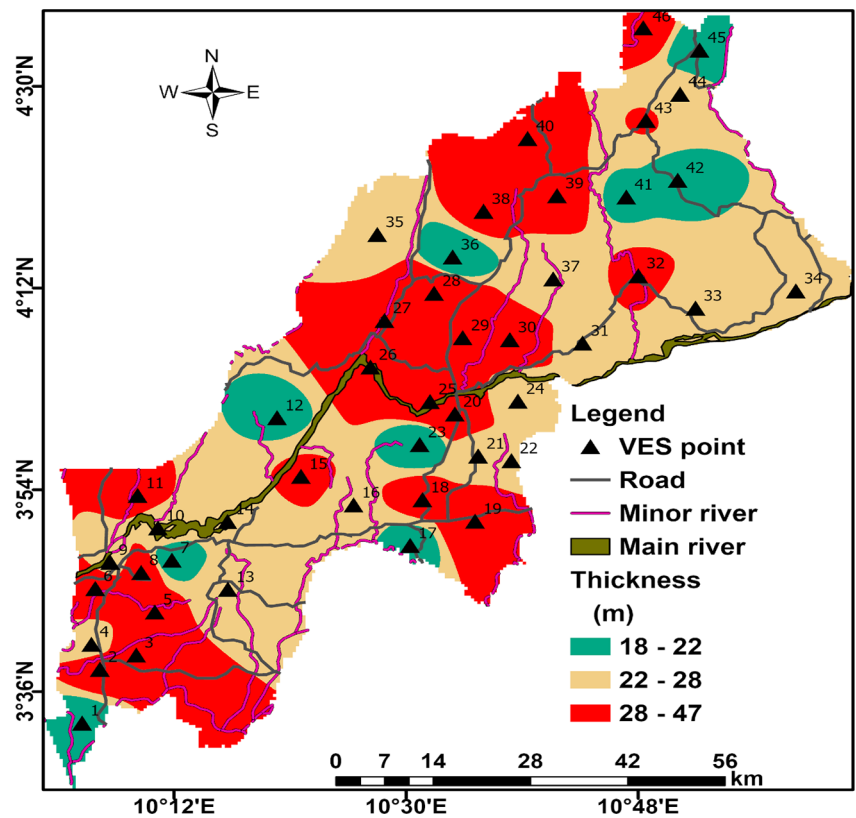


Fig. 9 Contour map for variation in aquifer thickness in the study area



aquifer characteristics within the study area. As per MacDonald et al. (2005), boreholes located near VES 1, 3, 20, and 22 exhibit moderate yields, ranging from 0.22 to 1.1 L/s, while the borehole near VES 30 demonstrates a high yield of

3.3 L/s. These borehole yield values further support the findings of aquifer transmissivity in the study area, as borehole yield serves as an indicator of aquifer transmissivity in basement complex settings (MacDonald et al. 2012).

Table 4 Estimated aquifer parameters from aquifer resistivity and thickness

VES No	$\rho_{aq}(\Omega m)$	h (m)	S (Ω^{-1})	T (Ωm^2)	K (m/day)	$T_r(m^2/day)$	Rc	Fc
1	3285.03	20.26	0.0062	66554.71	0.203	4.11	-0.222	0.637
2	1513.78	31.14	0.0206	47139.11	0.417	13.00	-0.548	0.292
3	230.37	39.94	0.1734	9200.98	2.417	96.54	-0.487	0.345
4	168.85	26.33	0.1559	4445.82	3.230	85.04	-0.466	0.364
5	4749.93	29.83	0.0063	141690.41	0.144	4.29	0.704	5.754
6	5620.92	40.08	0.0071	225286.47	0.123	4.92	0.266	1.723
7	96.74	20.48	0.2117	1981.24	5.680	104.62	-0.271	0.574
8	1434.34	26.25	0.0183	37651.43	0.439	11.52	0.492	2.938
9	1609.08	33.79	0.0210	54370.81	0.394	13.32	0.882	15.977
10	525.2	28.08	0.0535	14747.62	1.121	31.47	-0.084	0.845
11	2275.29	28.88	0.0127	65710.38	0.285	8.24	0.846	11.987
12	341	21.75	0.0638	7416.75	1.677	36.46	-0.370	0.460
13	517.34	23.95	0.0463	12390.29	1.136	27.22	-0.144	0.749
14	227.41	23.62	0.1039	5371.42	2.446	57.78	-0.178	0.697
15	373.9	28.59	0.0765	10689.80	1.538	43.99	-0.687	0.186
16	567.77	28.41	0.0500	16130.35	1.042	29.60	-0.572	0.272
17	482.57	20.91	0.0433	10090.54	1.213	25.36	0.778	8.020
18	1213.22	29.67	0.0245	35996.24	0.513	15.23	0.425	2.477
19	3336.4	40.81	0.0122	136158.48	0.200	8.15	0.934	29.518
20	16,500	42.57	0.0026	702405.00	0.045	1.91	0.798	8.900
21	347.7	23.71	0.0682	8243.97	1.646	39.04	-0.305	0.533
22	316.29	26.51	0.0838	8384.85	1.798	47.68	-0.692	0.182
23	1514.3	25.17	0.0166	38114.93	0.417	10.50	-0.279	0.564
24	325.72	19.45	0.0597	6335.25	1.750	34.03	-0.389	0.440
25	1600.49	43.39	0.0271	69445.26	0.396	17.20	0.635	4.477
26	123.15	34.5	0.2801	4248.68	4.335	149.57	-0.612	0.240
27	3634.66	29.13	0.0080	105877.65	0.184	5.37	-0.473	0.358
28	9817.89	46.69	0.0048	458397.28	0.073	3.41	0.711	5.925
29	6607.22	31.58	0.0048	208656.01	0.106	3.33	0.838	11.315
30	2613.64	32.05	0.0123	83767.16	0.251	8.04	0.512	3.102
31	2768.98	28.1	0.0101	77808.34	0.238	6.68	-0.554	0.287
32	145.51	28.67	0.1970	4171.77	3.710	106.38	-0.394	0.434
33	381.11	27.82	0.0730	10602.48	1.511	42.04	-0.645	0.216
34	524.31	28.09	0.0536	14727.87	1.122	31.53	-0.206	0.658
35	535	24.79	0.0463	13262.65	1.101	27.30	0.536	3.314
36	209.5	18.09	0.0863	3789.86	2.641	47.78	-0.322	0.512
37	179.4	22.77	0.1269	4084.94	3.052	69.50	-0.130	0.770
38	125.07	29.82	0.2384	3729.59	4.273	127.43	-0.175	0.702
39	316.63	31.99	0.1010	10128.99	1.797	57.47	-0.655	0.209
40	553.13	29.95	0.0541	16566.24	1.068	31.98	-0.211	0.651
41	104.85	21.82	0.2081	2287.83	5.037	109.91	-0.303	0.535
42	93.01	21.43	0.2304	1993.20	5.633	120.71	-0.543	0.296
43	307.77	28.51	0.0926	8774.52	1.845	52.59	-0.501	0.333
44	270.1	22.97	0.0850	6204.20	2.084	47.86	-0.496	0.337
45	135.49	19.45	0.1436	2635.28	3.966	77.13	-0.448	0.381
46	612.3	31.9	0.0521	19532.37	0.971	30.98	0.344	2.048
Mean	1722	29	0.076	60809	1.63	42.1	-0.059	2.86

The spatial variation of the reflection coefficient and fracture contrast in the study area are represented in Figs. 15 and 16, respectively. The reflection coefficient and fracture contrast serve as indicators for identifying water-filled fractures within the aquifer network (Obiora et al. 2016). The

presence of high density water-filled fractures is indicated in areas exhibiting reflection coefficients below 0.8 and fracture contrast values below 19 (Olayinka et al. 2000). Furthermore, areas with negative values of the reflection coefficient suggest a higher extent of fracturing. The

Fig. 10 Contour map showing the distribution of aquifer longitudinal conductance in the study area

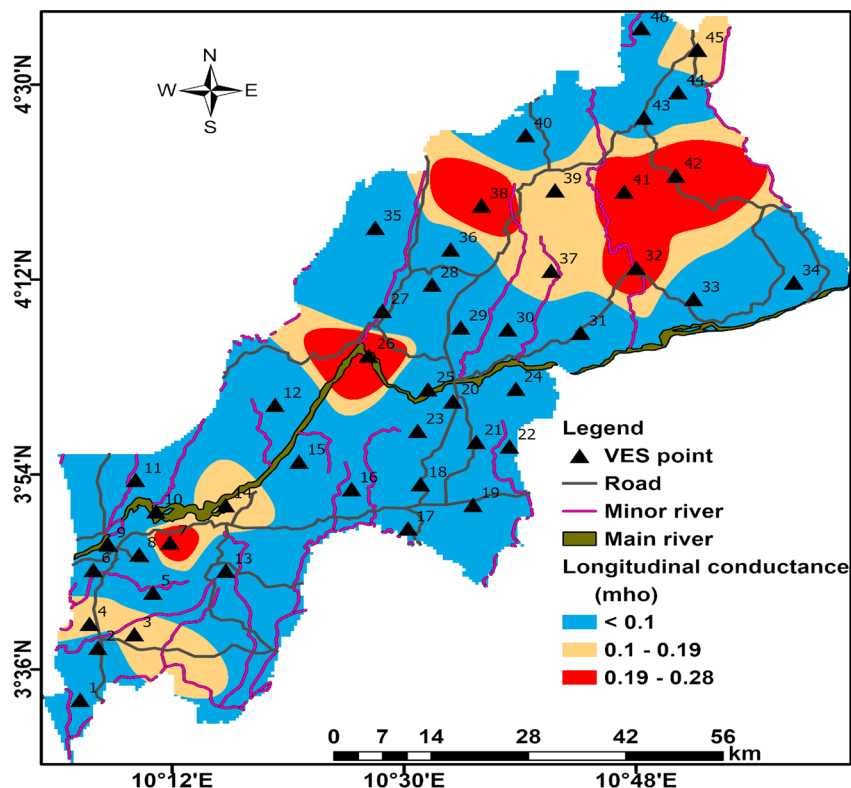
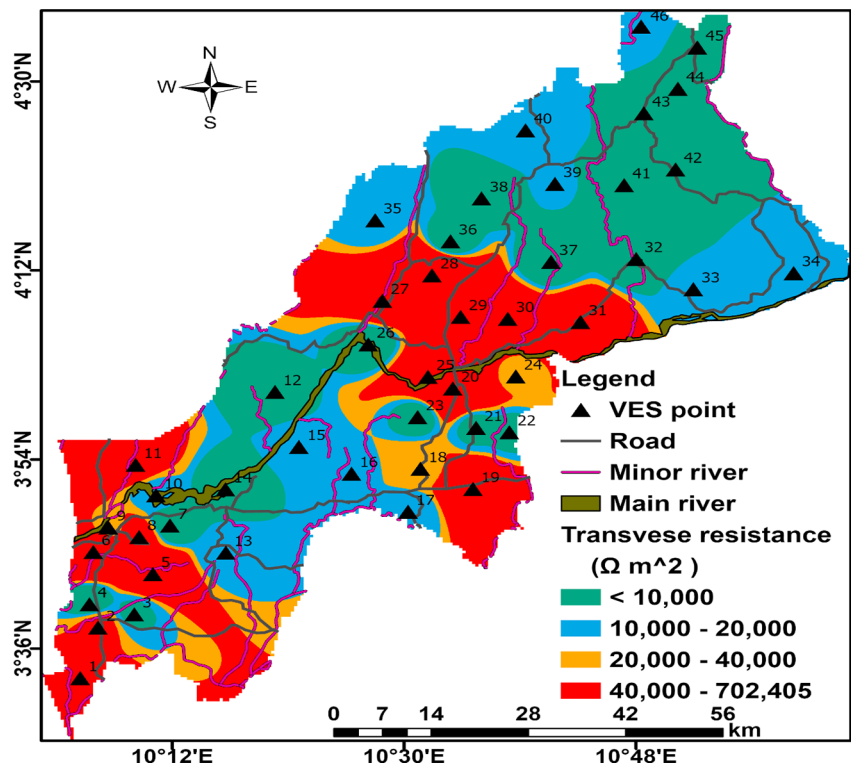


Fig. 11 Contour map for variation in transverse resistance in the study area



reflection coefficient in this study ranges from -0.67 to 0.93 with a mean of -0.059 , while the fracture contrast ranges from 0.19 to 29.5 , with a mean of 2.86 . The distribution of fracture contrast and reflection coefficient suggests that

the high degree of fracturing is localized in the northeastern parts of the study area. Groundwater potential in a basement complex relies on the aquifer resistivity, thickness, and transmissivity as well as the reflection coefficient and

Fig. 12 Contour map showing the distribution of hydraulic conductivity in the study area

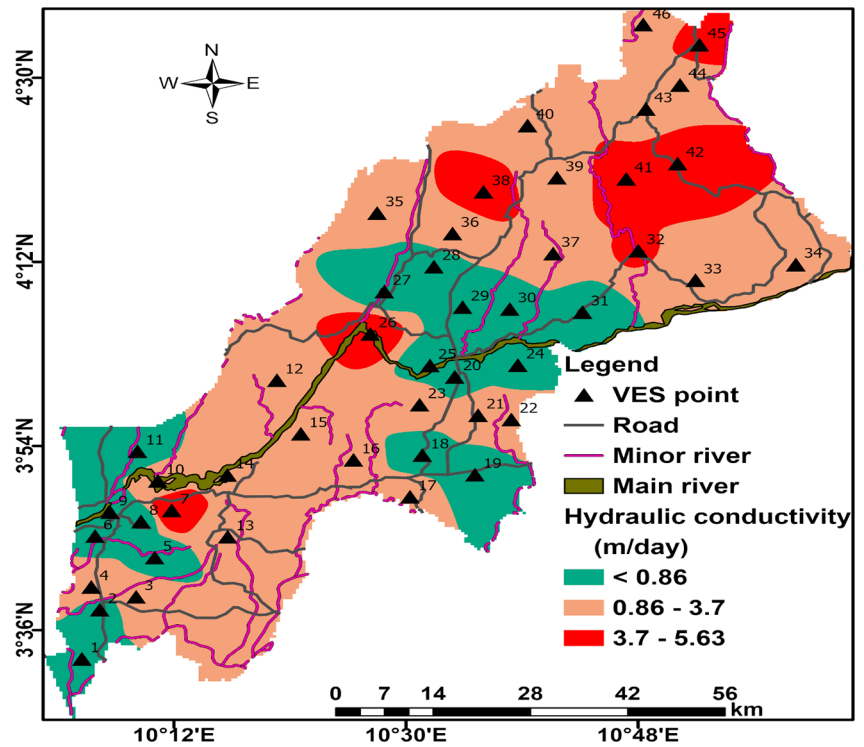
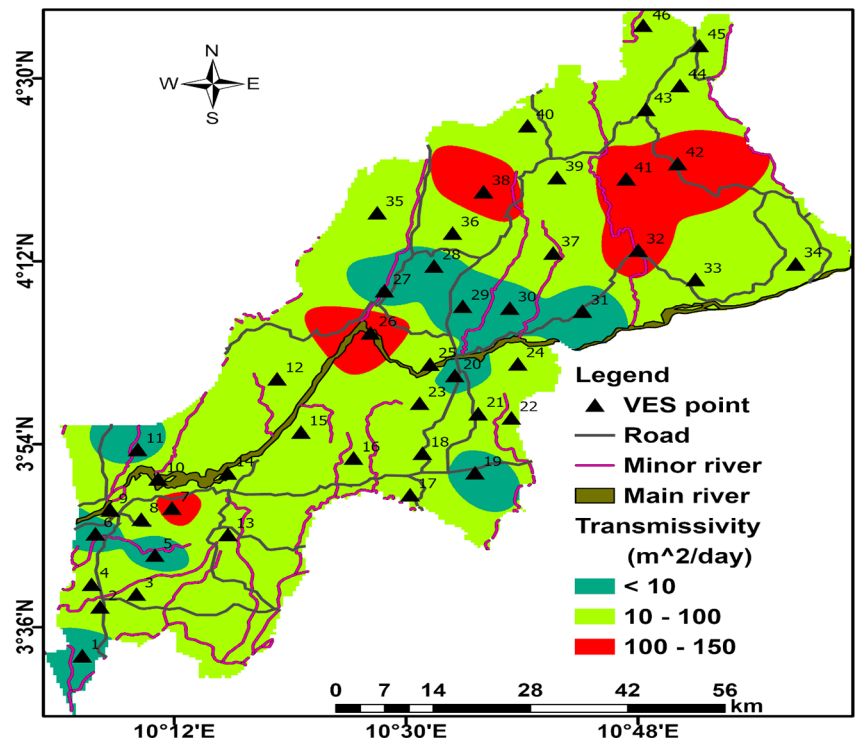


Fig. 13 Spatial distribution of aquifer transmissivity in the study area



fracture contrast (Raji and Abdulkadir 2020). This is because the aquifer recharge and discharge potential depends on the size of the aquifer, degree of fractures and the availability of water in the fractures. In this study, the spatial variation

of aquifer resistivity, transmissivity, reflection coefficient and fracture contrast are consistent. Based on this analysis, twenty-two VES points were identified as groundwater potentials of the study area (Table 6).

Fig. 14 Correlation between aquifer hydraulic conductivity and transmissivity

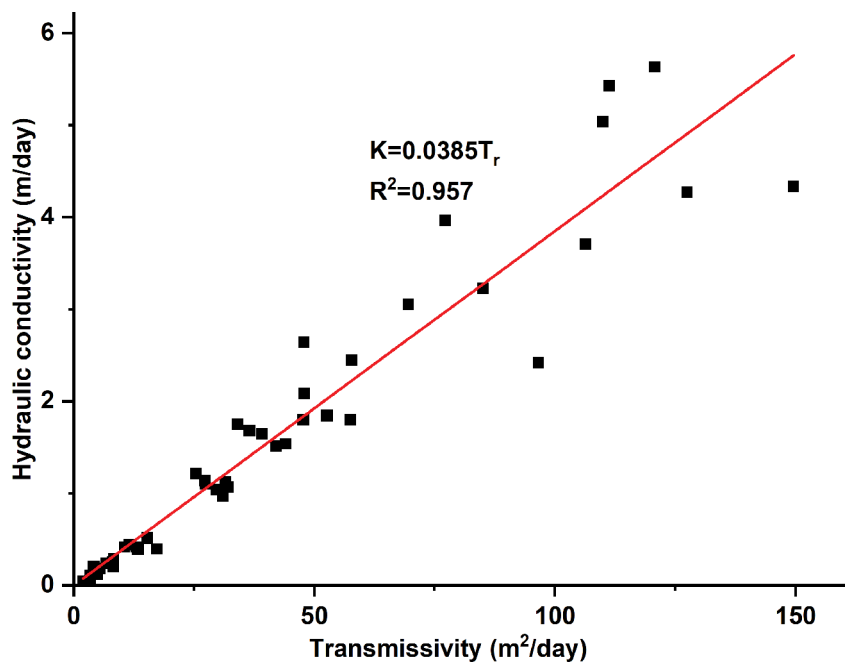


Table 5 Borehole parameters

Parameters	Borehole near VES 1	Borehole near VES 3	Borehole near VES 20	Borehole near VES 22	Borehole near VES 33
Depth (m)	45	40.00	75	40	42
Static water level (m)	5.30	4.45	4.55	3.70	3.81
Yield (L/second)	1.11	0.42	0.22	1.11	3.33
Drawdown (m)	3.52	10.97	0.60	1.78	6.77

Fig. 15 Contour map for variation in aquifer reflection coefficient in the study area

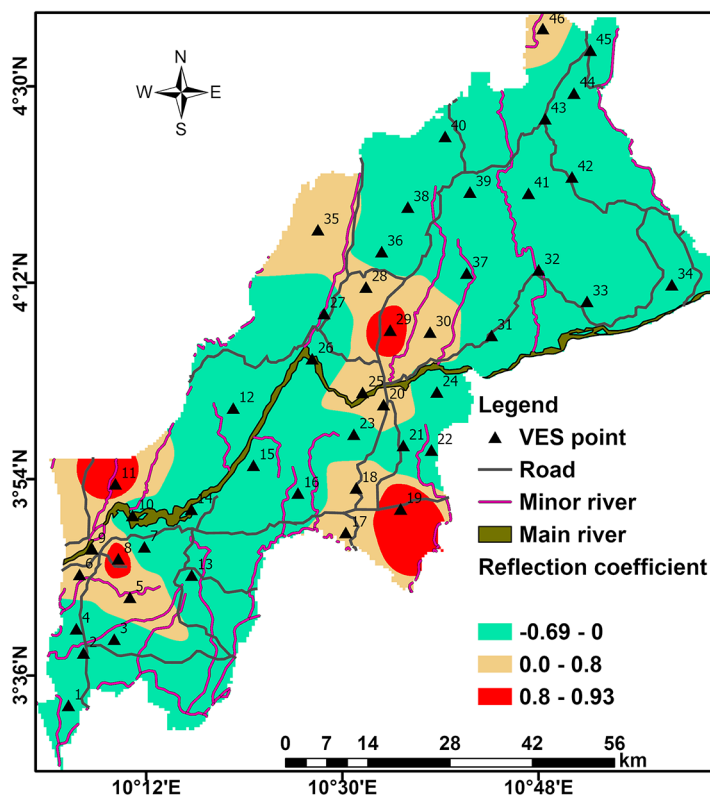


Fig. 16 Contour map showing the variation in fracture contrast in the study area

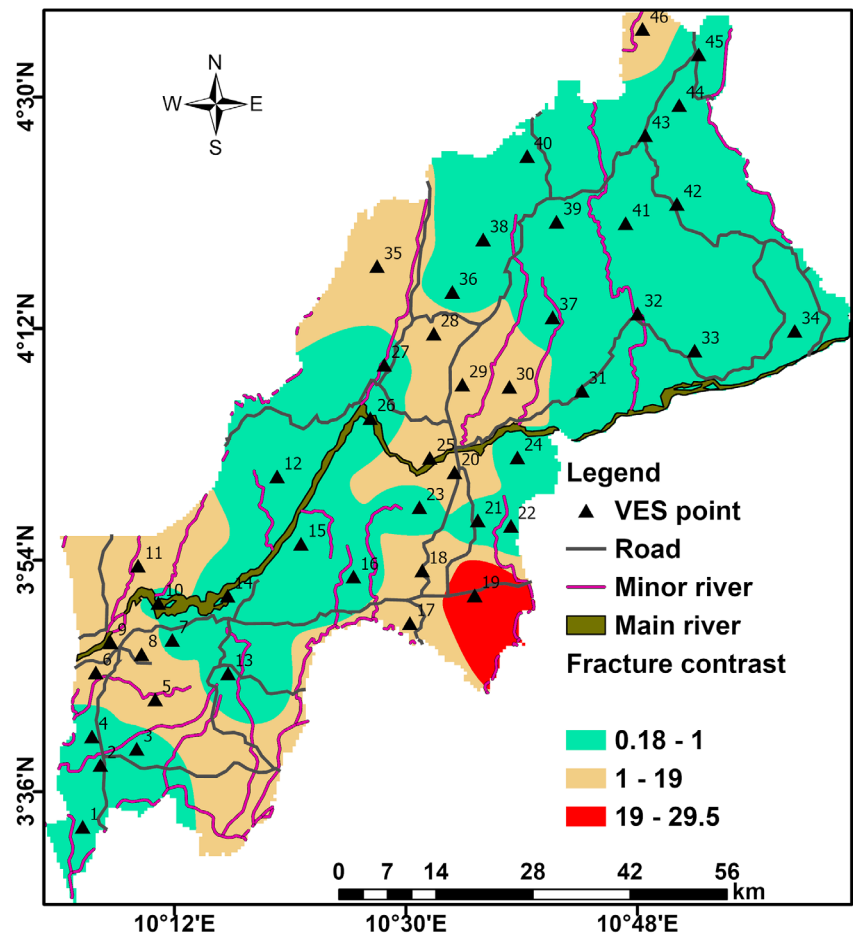


Table 6 Recommended groundwater potential areas

VES No	No of layers	Curve type	$\rho_{aq}(\Omega m)$	h (m)	Aquifer depth (m)	$T_r(m^2/day)$	R_c	F_c
3	4	KH	230	39.94	48.08	96.54	-0.487	0.345
4	5	HKH	168.85	26.33	33.61	85.04	-0.466	0.364
7	4	KH	96.74	20.48	34.94	104.62	-0.271	0.574
12	4	QH	341	21.75	33.71	36.46	-0.370	0.460
14	4	QH	227.41	23.62	33.77	57.78	-0.178	0.697
15	5	HKH	373.9	28.59	34.30	43.99	-0.687	0.186
17	4	HK	482.57	20.91	33.16	25.36	-0.778	8.020
21	4	QH	347.7	23.71	33.06	39.04	-0.305	0.533
22	4	KH	316.29	26.51	31.13	47.68	-0.692	0.182
24	4	KH	325.72	19.45	33.11	34.03	-0.389	0.440
26	4	QH	123.15	34.5	34.50	149.57	-0.612	0.240
32	4	QH	145.51	28.67	34.17	106.38	-0.394	0.434
33	4	KH	381.11	27.82	34.09	42.04	-0.645	0.216
36	4	KH	209.5	18.09	32.71	47.78	-0.322	0.512
37	4	QH	179.4	22.77	34.51	69.50	-0.130	0.770
38	3	H	125.07	29.82	34.29	127.43	-0.175	0.702
39	4	KH	316.63	31.99	34.07	57.47	-0.655	0.209
41	4	QH	104.85	21.82	36.65	109.91	-0.303	0.535
42	5	HKH	93.01	21.43	27.1	120.71	-0.543	0.296
43	4	KH	307.77	28.51	36.64	52.59	-0.501	0.333
44	4	KH	270.1	22.97	34.03	47.86	-0.496	0.337
45	4	QH	135.49	19.45	36.20	77.13	-0.448	0.381

Conclusion

This study employed the electrical resistivity technique to assess the groundwater potential in parts of the Sanaga maritime division where the development of groundwater through boreholes and wells has been plagued by a high rate of failure. To investigate the aquifer layer in the study area, the VES technique involving the Schlumberger electrode configuration was employed, and the obtained data were analyzed. Results from modeled sounding curves revealed that the subsurface consists of 3 to 5 geoelectric layers: top-soil, laterite, weathered formation, cracked gneiss and fresh/healthy gneiss. The sounding curves were best described as A, AA, H, HA, HK, HKH, KH, KHK, and QH, which revealed the heterogeneity of the subsurface in the study area. The third and fourth geoelectric layers with resistivity ranging from 93 to 16500 Ωm and thickness ranging from 18 to 47 m were identified as the aquifer unit of the study area. These parameters were used to evaluate the aquifer characteristics including the longitudinal conductance, transverse resistance, hydraulic conductivity, transmissivity, reflection coefficient and fracture contrast. The hydraulic conductivity ranged from 0.05 to 5.67 m/day with a mean of while the transmissivity ranged from 2 to 150 m^2/day with an average value of 42.1 m^2/day . The transmissivity and hydraulic conductivity revealed that the groundwater potential of the study area is generally moderate. The reflection coefficient and fracture contrast revealed that the study area generally has high density water-bearing fractures with a high degree of fracturing in the northeastern parts. Twenty-two VES points were recommended as aquifer potentials of the study area with aquifer resistivity and thickness that vary from 93–47 Ωm and 19–40 m, respectively. The hydrogeological units of the study area showed poor, weak and moderate aquifer protective capacity with values ranging from 0.0026 to 0.28 mhos

Acknowledgements We would like to thank the team and sponsors of this geophysical campaign, with special recognition to Dr. Blaise P. Gounou Pokam for generously providing the data that was utilized in this study.

Data availability Data could be provided upon request.

Declarations

Conflict of interest Authors declare that there is no conflict of interest.

References

- Abdelrahman K, Hazaea SA, Hazaea BY, Abioui M, Al-Awah H (2023) Groundwater potentiality in hard-rock terrain of southern Saudi Arabia using electrical resistivity tomography approach. *King Saud Univ Sci* 35:102928. <https://doi.org/10.1016/j.jksus.2023.102928>
- Adeyemo IA, Omosuyi GO, Ojo BT, Adekunle A (2017) Groundwater potential evaluation in a typical basement Complex Environment using GRT Index—A Case Study of Ipinso-Okeodu Area, near Akure, Nigeria. *J Geosci Environ Prot* 05:240–251. <https://doi.org/10.4236/gep.2017.53017>
- Bello HI, Alhassan UD, Salako KA, Rafiu AA, Adetona AA, Shehu J (2019) Geoelectrical investigation of groundwater potential, at Nigerian Union of Teachers Housing estate, Paggo, Minna, Nigeria. *Appl Water Sci* 9:52. <https://doi.org/10.1007/s13201-019-0922-z>
- Bon AF, Ombolo A, Biboum PM, Moutlen JM, Mboudou GE (2022) Identification of hydrogeological features using remote sensing and electromagnetic methods in the hard-rock formations of the Cameroon coastal plain (Central Africa): implications for water borehole location. *Sci Afr* 17:e01272. <https://doi.org/10.1016/j.sciaf.2022.e01272>
- Bondje LMNB, Betsi TB, Nga LNYM, Belnoun RNN, Molotouala AC, McFarlane C, Bitom LD (2020) Geochemistry of rutile from the pan-african Yaoundé metamorphic group: implications for provenance and conditions of formation. *J Afr Earth Sci*. <https://doi.org/10.1016/j.jafrearsci.2020.103912>
- Chow VT, Maidment DR, Mays LW (1988) *Applied Hydrology*. McGraw-Hill, New York
- Dan-Hassan MA, Olorunfemi MO (1999) Hydro-geophysical investigation of a basement terrain in the north-central part of Kaduna State, Nigeria. *J Min Geol* 33(2):189–206
- Datta A, Gaikwad H, Kadam A, Umrikar BN (2020) Evaluation of groundwater prolific zones in the unconfined basaltic aquifers of Western India using geospatial modeling and MIF technique. *Model Earth Syst Environ* 6:1807–1821. <https://doi.org/10.1007/s40808-020-00791-0>
- Dhinsa D, Tamiru F, Tadesa B (2022) Groundwater potential zonation using VES and GIS techniques: a case study of Weserbi Guto catchment in Sululta. *Oromia Ethiopia Heliyon* 8:e10245. <https://doi.org/10.1016/j.heliyon.2022.e10245>
- Dumort JC (1968) Carte géologique de reconnaissance de la République Fédérale Du Cameroun Au 1/500000, vol Feuille NB 32 SE 028. Direction des mines et de la géologie
- Ebong ED, Abong AA, Ulem EB, Ebong LA (2021) Geoelectrical Resistivity and Geological characterization of hydrostructures for Groundwater Resource Appraisal in the Obudu Plateau, Southeastern Nigeria. *Nat Resour Res* 30:2103–2117. <https://doi.org/10.1007/s11053-021-09818-4>
- Ekanem AM (2020) Georesistivity modelling and appraisal of soil water retention capacity in Akwa Ibom State University main campus and its environs, Southern Nigeria. *Modelling Earth Syst Environ* 6:2597–2608. <https://doi.org/10.1007/s40899-020-00467-8>
- Ekanem AM, George NJ, Thomas JE, Nathaniel EU (2020) Empirical relations between Aquifer Geohydraulic–Geoelectric Properties Derived from Surficial Resistivity Measurements in Parts of Akwa Ibom State, Southern Nigeria. *Nat Resour Res* 29:2635–2646. <https://doi.org/10.1007/s11053-019-09606-1>
- Ekine AS, Osobonye GT (1996) Surface geoelectric sounding for the determination of Aquifer characteristics in parts of Bonny Local Government Area, Rivers State, Nigeria. *Niger J Phys* 85:93–97
- Eugene-Okorie JO, Obiora DN, Ibuot JC, Ugbor DO (2020) Geoelectrical investigation of groundwater potential and vulnerability of Oraifite, Anambra State, Nigeria. *Appl Water Sci* 10:223. <https://doi.org/10.1007/s13201-020-01304-1>
- Evans UF, George NJ, Akpan AE, Obot IB, Ikot AN (2010) A study of superficial sediments and aquifers in parts of Uyo Local Government Area, Akwa Ibom State, Southern Nigeria, using electrical sounding method. *E-J Chem* 7(3):1018–1022. <https://doi.org/10.1155/2010/975965>

- George NJ, Ibuot JC, Obiora DN (2015) Geoelectrohydraulic parameters of shallow sandy aquifer in Itu, Akwa Ibom State (Nigeria) using geoelectric and hydrogeological measurements. *J Afr Earth Sci* 110:52–63. <https://doi.org/10.1016/j.jafrearsci.2015.06.006>
- George NJ, Akpan AE, Evans UF (2016) Prediction of geohydraulic pore pressure gradient differentials for hydrodynamic assessment of hydrogeological units using geophysical and laboratory techniques: a case study of the coastal sector of Akwa Ibom State, Southern Nigeria. *Arab J Geosci* 9:305. <https://doi.org/10.1007/s12517-016-2337-6>
- Heigold PC, Gilkeson RH, Cartwright K, Reed PC (1979) Aquifer Transmissivity from Surficial Electrical methods. *Groundwater* 17(4):338–345. <https://doi.org/10.1111/j.1745-6584.1979.tb03326.x>
- Iserhien-Emekeme R, Ofomola MO, Bawallah M, Anomohanran O (2017) Lithological identification and underground water conditions in Jeddo using geophysical and geochemical methods. *Hydrology* 4:42. <https://doi.org/10.3390/hydrology4030042>
- Jude PN, Victor JK, Pierre W, Anoh NO, Abasoh ME, Rosvelt MDM, Tabod TC (2021) Petrographic, morpho-structural and geophysical study of the quartzite deposit in the central part of Pouma, Littoral-Cameroon. *Results Geophys Sci* 7:100019. <https://doi.org/10.1016/j.ringsps.2021.100019>
- Kirsch R (2009) *Groundwater Geophysics: A Tool for Hydrogeology*. Berlin, Germany. <https://doi.org/10.1007/978-3-540-88405-7>
- Koji E, Noah Ewoti OV, Onana FM, Tchakonté S, Djimeli CL, Arfao AT, Bricheux G, Sime-Ngando T, Nola M (2017) Influence of Anthropogenic Pollution on the Abundance Dynamics of some Freshwater Invertebrates in the Coastal Area of Cameroon. *J Environ Prot* 08:810–829. <https://doi.org/10.4236/jep.2017.87051>
- Konwea C, Ajayi O (2021) Effectiveness of different Hand-Dug Well Treatment methods in a typical basement Complex Environment. *J Min Geol* 57(2):331–337
- Konwea CI, Evurani DE, Ajayi O (2023) Assessment of groundwater potential of the Obafemi Awolowo University Estate, Southwestern Nigeria. *Sci Afr* 20:e01597. <https://doi.org/10.1016/j.sciaf.2023.e01597>
- Krasny (1993) Classification of transmissivity magnitude and variation. *Groundwater* 31(2):230–236. <https://doi.org/10.1111/j.1745-6584.1993.tb01815.x>
- Lavenir JMN, Cyrille S, Paul NJ, Suh CE (2019) Structural characterization of Outcrop-Scale in Edea and Eséka Area: evidence for a Complex Polyphase Deformation in the Paleoproterozoic Nyong Serie (Congo Craton-South Cameroon). *IOSR J Appl Geol Geophys* 7(5):1–9. <https://doi.org/10.9790/0990-0705010109>
- Lerouge C, Cocherie A, Toteu SF, Penaye J, Milési JP, Tchameni R, Nsifa EN, Mark Fanning C, Deloule E (2006) Shrimp U-Pb zircon age evidence for paleoproterozoic sedimentation and 2.05 Ga syntectonic plutonism in the Nyong Group, South-Western Cameroon: consequences for the Eburnean-Transamazonian belt of NE Brazil and Central Africa. *J Afr Earth Sci* 44:413–427. <https://doi.org/10.1016/j.jafrearsci.2005.11.010>
- MacDonald A, Davies J, Calow R, Chilton J (2005) *Developing groundwater: A Guide for Rural Water Supply*. Warwickshire, UK. <https://doi.org/10.3362/9781780441290>
- MacDonald A, Bonsor H, Dochartaigh B, Taylor RG (2012) Quantitative maps of groundwater resources in Africa. *Environ Res Lett* 7:024009. <https://doi.org/10.1088/1748-9326/7/2/024009>
- Maillet R (1947) The fundamental equations of electrical prospecting. *J Gen Appl Geophys* 12(4):529–556. <https://doi.org/10.1190/1.1437342>
- Mimba ME, Tamnta NM, Suh CE (2014) Geochemical Dispersion of Gold in Stream Sediments in the Paleoproterozoic Nyong Series, Southern Cameroon. *Sci Res* 2(6):155–165. <https://doi.org/10.11648/j.sr.20140206.12>
- Mogaji KA, Omobude OB (2017) Modeling of geoelectric parameters for assessing groundwater potentiality in a multifaceted geologic terrain, Ipinsa Southwest, Nigeria – A GIS-based GODT approach. *NRIAG J Astron Geophys* 6(2):434–451. <https://doi.org/10.1016/j.nrjag.2017.07.001>
- Nédélec A, Minyem D, Barbey P (1993) High-P-high-T anatexis of archaean tonalitic grey gneisses: the Eséka migmatites, Cameroon. *Precambrian Res* 62(3):191–205. [https://doi.org/10.1016/0301-9268\(93\)90021-S](https://doi.org/10.1016/0301-9268(93)90021-S)
- Nga EN, Kidik Pouka C, Ngo Boumsong PC, Dibong SD, Mpondo Mpondo E (2016) Inventaire et caractérisation des plantes médicinales utilisées en thérapeutique dans le département de la Sanaga Maritime: ndom, Ngambe et Pouma. *J Appl Biosci* 106:10333–10352. <https://doi.org/10.4314/jab.v106i1.13>
- Niwas S, Singhal DC (1981) Estimation of aquifer transmissivity from Dar-Zarrouk parameters in porous media. *J Hydrol* 50:393–399. [https://doi.org/10.1016/0022-1694\(81\)90082-2](https://doi.org/10.1016/0022-1694(81)90082-2)
- Noiha V, Zapfack L, Mbade L (2015) Biodiversity Management and Plant Dynamic in a Cocoa Agroforest (Cameroon). *Int J Plant Soil Sci* 6(2):101–108. <https://doi.org/10.9734/ijpss/2015/10347>
- Nzeket AB, Moyo KB, Aboubakar A, Youdom YAS, Moussima YDA, Zing ZB, Sulem YNN, Anselme Crépin M, Mfopou MYC (2019) Assessment of Physicochemical and Heavy Metal Properties of Groundwater in Edéa (Cameroon). *Am J Water Resour* 7(1):1–10. <https://doi.org/10.12691/ajwr-7-1-1>
- Obiora DN, Ibuot JC, George NJ (2016) Evaluation of aquifer potential, geoelectric and hydraulic parameters in Ezza North, south-eastern Nigeria, using geoelectric sounding. *Int J Environ Sci Technol* 13:435–444. <https://doi.org/10.1007/s13762-015-0886-y>
- Obiora DN, Ibuot JC, Alhassan UD, Okeke FN (2017) Study of aquifer characteristics in northern Paiko, Niger State, Nigeria, using geoelectric resistivity method. *Int J Environ Sci Technol* 15:2423–2432. <https://doi.org/10.1007/s13762-017-1612-8>
- Oguama BE, Ibuot JC, Obiora DN, Aka MU (2019) Geophysical investigation of groundwater potential, aquifer parameters, and vulnerability: a case. (Technical) *Model Earth Syst Environ* 5:1123–1133. <https://doi.org/10.1007/s40808-019-00595-x>. study of Enugu State College of Education
- Okpoli CC, Ozomoge P (2020) Groundwater exploration in a typical southwestern basement terrain. *NRIAG J Astron Geophys* 9(1):289–308. <https://doi.org/10.1080/20909977.2020.1742441>
- Olabanji OA, Akinlabi JO, Olusegun AO, Adedirán A (2019) Investigating Groundwater Challenge in Crystalline Basement Complex Terrain of South-Western Nigeria: Case Study of Aagba and Environs. *Int J Res Rev* 6(2):58–68. <https://www.researchgate.net/publication/341160648>
- Oladapo MI, Akintorinwa OJ (2007) Hydrogeophysical Study of Ogbese South Western Nigeria. *Glob J Pure Appl Sci* 13(1):55–61
- Oladunjoye MA, Adefehinti A, Ganiyu K, AO (2018) Geophysical appraisal of groundwater potential in the crystalline rock of Kishi area, Southwestern Nigeria. *J Afr Earth Sci*. <https://doi.org/10.1016/j.jafrearsci.2018.11.017>
- Olayinka AI (1996) Non uniqueness in the interpretation of bedrock resistivity from sounding curve and its hydrological implications. *Water Resour J* 7(1–2):55–60
- Olayinka AI, Obere F, David L (2000) Estimation of longitudinal resistivity from Schlumberger sounding curves. *J Min Geol* 36(2):225–242
- Olorunfemi MO, Fasuyi SA (1993) Aquifer types and the geoelectric/hydrogeologic characteristics of part of the central basement terrain of Nigeria (Niger State). *J Afr Earth Sci* 16(3):309–317. [https://doi.org/10.1016/0899-5362\(93\)90051-Q](https://doi.org/10.1016/0899-5362(93)90051-Q)
- Omosuyi GO (2010) Geoelectric assessment of groundwater prospect and vulnerability of overburden aquifers at Idanre, Southwestern Nigeria. *Ozean J Appl Sci* 3(19):28

- Omosuyi GO, Oshodi DR, Sanusi SO, Adeyemo IA (2020) Groundwater potential evaluation using geoelectrical and analytical hierarchy process modeling techniques in Akure-Owode, southwestern Nigeria. *Model Earth Syst Environ* 7:145–158. <https://doi.org/10.1007/s40808-020-00915-6>
- Ossai MN, Okeke FN, Obiora DN, Ibuot JC (2023) Evaluation of groundwater repositories in parts of Enugu, Eastern Nigeria via electrical resistivity technique. *Appl Water Sci* 13:64. <https://doi.org/10.1007/s13201-022-01839-5>
- Rajendran G, Mohammed M, Shivakumar S, Merera W, Taddese K (2020) Geospatial techniques amalgamated with two-dimensional electrical resistivity imaging for delineation of groundwater potential zones in West Guji Zone, Ethiopia. *Groundw Sustain Dev* 11:100407. <https://doi.org/10.1016/j.gsd.2020.100407>
- Raji WO, Abdulkadir KA (2020) Evaluation of groundwater potential of bedrock aquifers in geological sheet 223 Ilorin, Nigeria, using geo-electric sounding. *Appl Water Sci* 10:220. <https://doi.org/10.1007/s13201-020-01303-2>
- Raji WO, Abdulkadir KA (2022) Quantitative estimates of groundwater resource parameters in non-sedimentary aquifers of Northcentral Nigeria. *J Afr Earth Sci* 196:104695. <https://doi.org/10.1016/j.jafrearsci.2022.104695>
- Rodrigue TT, Victor KJ, Lucas K, Adoua NK, Le-sage KTM, Stéphane TT (2022) Contribution of vertical electrical soundings, landsat 8 and SRTM images to the comparative study of the hydrogeological characteristics of the Foto, Keleng and Foreké areas, West Cameroon. *Heliyon* 8:e09675. <https://doi.org/10.1016/j.heliyon.2022.e09675>
- Roy A, Apparao A (1971) Depth of investigation in Direct current methods. *Geophysics* 36(5):943–959
- Salako KA, Adetona AA, Rafiu AA, Ofor NP, Alhassan UD, Udensi EE (2009) Vertical electrical sounding investigation for groundwater at the southwestern part (site A) of Nigeria Mobile Police barracks (MOPOL 12), David Mark road, Maitumbi, Minna. *J Sci Educ Technol* 2(1):350–362
- Shang CK, Satir M, Nsifa EN, Liégeois JP, Siebel W, Taubald H (2007) Archaean high-K granitoids produced by remelting of earlier Tonalite-Trondhjemite-Granodiorite (TTG) in the Sangmelima region of the Ntem complex of the Congo craton, southern Cameroon. *Int J Earth Sci* 96(5):817–841. <https://doi.org/10.1007/s00531-006-0141-3>
- Sirhan A, Hamidi M, Andrieux P (2011) Electrical resistivity tomography, an assessment tool for water resource: case study of Al-Aroub Basin, West Bank, Palestine. *Asian J Earth Sci* 4:38–45. <https://doi.org/10.3923/ajes.2011.38.45>
- Stendal H, Toteu SF, Frei R, Penaye J, Njel UO, Bassahak J, Nni J, Kankeu B, Ngako V, Hell JV (2006) Derivation of detrital rutile in the Yaoundé region from the neoproterozoic pan-african belt in southern Cameroon (Central Africa). *J Afr Earth Sci* 44(4–5):443–458. <https://doi.org/10.1016/j.jafrearsci.2005.11.012>
- Tang SN, Etame J, Bayiga E, Gérard M, Bilong P (2012) Negative europium anomalies in a lateritic profile over gneiss at Edea (coastal plain, Cameroon). *RevCAMES-Série A* 13(1):97–102
- Tchindjang M, Saha F, Levang P, Voundi E, Njombissie PCI, Minka F (2016) Palmeraies élitistes et villageoises et développement socioéconomique dans la sanaga maritime: impacts, conséquences et perspectives. *Revue Scientifique et Technique Forêt et Environnement Du Bassin Du Congo* 7:37–52
- Tepoule N, Kenfack JV, Ndikum Ndohe E, Koumetio F, Tabod TC (2022) Delineation of groundwater potential zones in Logbadejeck, Cameroun: an integrated geophysical and geospatial study approach. *Int J Environ Sci Technol* 19:2039–2058. <https://doi.org/10.1007/s13762-021-03259-5>
- Teutsong T, Temga JP, Enyegue AA, Feuwo NN, Bitom D (2021) Petrographic and geochemical characterization of weathered materials developed on BIF from the Mamelles iron ore deposit in the Nyong unit, South-West Cameroon. *Acta Geochim* 40:163–175. <https://doi.org/10.1007/s11631-020-00421-7>
- Tonga C, Kimbi HK, Anchang-Kimbi JK, Nyabeyeu HN, Bisse-mou ZB, Lehman LG (2013) Malaria risk factors in women on intermittent preventive treatment at delivery and their effects on pregnancy outcome in Sanaga-Maritime, Cameroon. *PLoS ONE* 8:e65876. <https://doi.org/10.1371/journal.pone.0065876>
- Toteu SF, Van Schmus WR, Penaye J, Nyobé JB (1994) UPb and SmN evidence for Eburnian and pan-african high-grade metamorphism in cratonic rocks of southern Cameroon. *Precambrian Res* 67:321–347. [https://doi.org/10.1016/0301-9268\(94\)90014-0](https://doi.org/10.1016/0301-9268(94)90014-0)
- Toteu SF, Penaye J, Deloule E, Van Schmus WR, Tchameni R (2006) Diachronous evolution of volcano-sedimentary basins north of the Congo craton: insights from U-Pb ion microprobe dating of zircons from the Poli, Lom and Yaoundé groups (Cameroon). *Afr Earth Sci* 44(4–5):428–442. <https://doi.org/10.1016/j.jafrearsci.2005.11.011>
- Victor M, Charles N, Jacqueline TN, Daniel N (2014) Application of Remote sensing for the Mapping of Geological structures in Rainforest Area: a case study at the Matomb-Makak Area, Center-South Cameroon. *J Geosci Geomat* 2(5):196–207. <https://doi.org/10.12691/jgg-2-5-3>
- Vuorinen HS, Juuti PS, Katko TS (2007) History of water and health from ancient civilizations to modern times. *Water Sci Technology: Water Supply* 7(1):49–57. <https://doi.org/10.2166/ws.2007.006>
- Yonta-Ngoune C, Nkoumbou C, Barbey P, Le Breton N, Montel JM, Villieras F (2010) Geological context of the Boumnyebel talcschists (Cameroun): inferences on the pan-african Belt of Central Africa. *C R Geosci* 342(2):108–115. <https://doi.org/10.1016/j.crte.2009.12.007>
- Zohdy AA, Eaton GP, Mabey DR (1974) Application of Surface Geophysics to Ground-Water investigations: techniques of water resources investigations of U.S. Geol. Survey. U.S. Government Printing Office, Washington, p 66

Publisher's Note Springer Nature remains neutral with regard to jurisdictional claims in published maps and institutional affiliations.

Springer Nature or its licensor (e.g. a society or other partner) holds exclusive rights to this article under a publishing agreement with the author(s) or other rightsholder(s); author self-archiving of the accepted manuscript version of this article is solely governed by the terms of such publishing agreement and applicable law.